Inorganic Chemistry

Article

pubs.acs.org/IC

Re(I) Complexes of Substituted dppz: A Computational and Spectroscopic Study

Holly van der Salm,[†] Michael G. Fraser,[†] Raphael Horvath,[‡] Scott A. Cameron,[†] Jonathan E. Barnsley,[†] Xue-Zhong Sun,[‡] Michael W. George,*[,‡] and Keith C. Gordon*

[†]Department of Chemistry, University of Otago, Union Place, 9016 Dunedin, New Zealand

[‡]School of Chemistry, University of Nottingham, Nottingham NG7 2NR, United Kingdom

Supporting Information

ABSTRACT: A series of dipyrido[3,2-*a*:2′,3′-*c*]phenazine (dppz)-based ligands with electron-withdrawing substituents and their $[Re(CO)_3(L)Cl]$ and $[Re(CO)_3(L)(py)]PF_6$ complexes have been studied using Raman, resonance Raman, and transient resonance Raman (TR^2) and time-resolved infrared (TRIR) spectroscopic techinques in conjunction with computational chemistry as well as electrochemical studies, emission, and absorption of ground and excited states. DFT (B3LYP) frequency calculations show good agreement with nonresonant Raman spectra, which allowed these to be used to identify phenanthroline, phenazine, and delocalized modes. These band assignments were used to establish the nature of chromophores active in resonance Raman spectra, probed with wavelengths between 350.7 and 457.9 nm. X-ray crystallography of $[Re(CO)_3(dppzBr_2)Cl]$ and $[Re(CO)_3(dppzBr)(py)]PF_6$ showed these crystallize in space groups triclinic *P*1 and monoclinic $P2_{1/n}$, respectively. Electrochemical studies showed that substituents have a strong effect on the phenazine MO, changing the reduction potential by 200 mV. Transient absorption studies showed that generally the $[Re(CO)_3(L)(py)]PF_6$ complexes had longer lifetimes than the corresponding $[Re(CO)_3(L)Cl]$ complexes; the probed state is likely to be $^3\pi \rightarrow \pi^*$ (phz) in nature. TR^2 spectra of the ligands provided a marker for the triplet $\pi \rightarrow \pi^*$ state, and the TR^2 spectra of the complexes suggest an intraligand (IL) π,π^* state for $[Re(CO)_3(L)(py)]^+$ complexes, and a potentially mixed IL/MLCT state for $[Re(CO)_3(L)Cl]$ complexes. TRIR spectroscopy is more definitive with THEXI state assignments, and analysis of the metal−carbonyl region (1800−2100 cm^{-1}) on the picosecond and nanosecond time scales indicates the formation of MLCT(phen/phz) states for all $[Re(CO)_3(L)Cl]$ complexes, and IL $\pi \rightarrow \pi^*$ (phen) states for all $[Re(CO)_3(L)(py)]^+$ complexes, with all but $[Re(CO)_3(dppzBr(CF_3))(py)]^+$ showing some contribution from an MLCT(phen) state also.

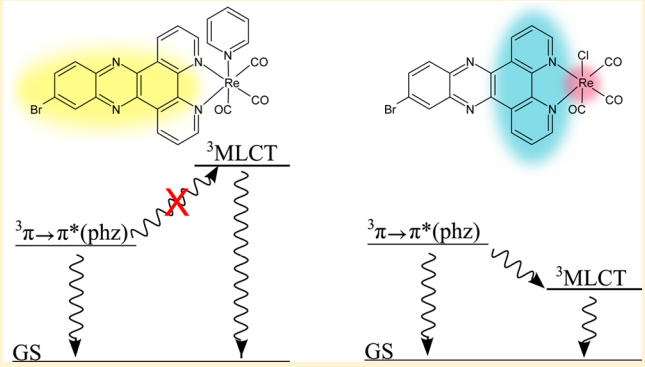

INTRODUCTION

The dipyrido[3,2-*a*;2′,3′-*c*]phenazine (dppz) ligand, its derivatives, and its complexes have been extensively studied because of their interesting photophysical properties,[1−4] which also make them potentially useful for a range of applications.[5,6] Some dppz complexes, such as $[Ru(bpy)_2(dppz)]^{2+}$, exhibit the "light-switch" effect, where they are nonemissive in aqueous solution or protic solvents but highly emissive in aqueous solutions when DNA is present or in aprotic solvents.[7−10] Many studies, both photophysical and theoretical, have suggested that Re(I)−and Ru(II)−dppz complexes show two low-lying triplet metal to ligand charge-transfer (MLCT) states and one triplet ligand-centered state.[11−13] The MLCT state may be distinguished as one that populates the phenazine-like molecular orbital (MO) (Figure 1a), while the other populates the phenanthroline-like MO (Figure 1b). The ^{3}MLCT (phen) state is emissive, while the ^{3}MLCT (phz) state is a dark state. The emissive behavior was previously explained by an interplay between the two ^{3}MLCT states, depending on which state was stabilized by the environment.[14] It was thought that in protic solvents hydrogen bonding to phenazine nitrogens stabilized the dark ^{3}MLCT (phz) state, while this did not occur when intercalated to DNA or in aprotic solvents, and the phz state was less stable, leaving the ^{3}MLCT (phen) emissive state lower in energy.[15]

However, Brennaman et al.[8] showed using temperature-dependent lifetime measurements of $[Ru(bpy)_2(dppz)]^{2+}$ excited states in different solvents that it is unlikely the MLCT (phen) (bright state) and MLCT (phz) (dark state) change in energy with environment, but rather the dark (MLCT (phz)) is enthalpically favored, while the bright state is entropically favored, and competition between these factors determines whether the compound is emissive or not. The relevant unoccupied molecular orbitals (see Figure 1) are very close in energy, and their ordering may be affected by

Received: December 17, 2013
Published: February 21, 2014

   dx.doi.org/10.1021/ic403056g | *Inorg. Chem.* 2014, 53, 3126−3140

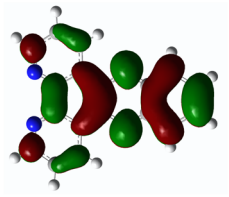

(a) dppz LUMO, b_1(phz)

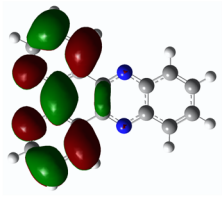

(b) dppz L+2, b_1(phen)

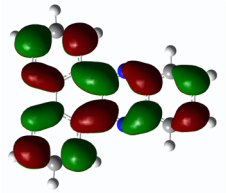

(c) dppz L+1, a_2

Figure 1. Three lowest energy unoccupied molecular orbitals in dppz and their symmetry calculated with B3LYP functional in vacuo.

substitution or by chelation to a metal center. Electron-withdrawing substituents are used, as has previously been observed, to potentially perturb the partitioning between the phen and phz molecular orbitals. These systems offer additional synthetic utility in that they can alter the balance of MOs, but may be additionally decorated using coupling chemistry.[16] In this paper, a series of dppz-based ligands and a pyrido-[2′,3′:5,6]pyrazino[2,3-*f*][1,10]phenanthroline (ppp)-based ligand with electron-withdrawing substituents are reported (see Figure 2). The ground- and excited-state properties were investigated using a variety of spectroscopic methods in concert with density functional theory (DFT) calculations.

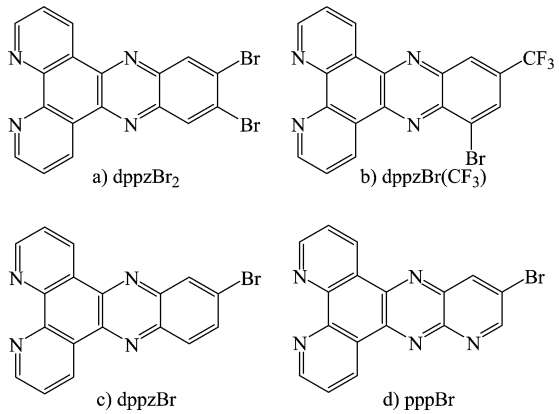

Figure 2. Substituted dppz-based and ppp-based ligands presented in this study.

EXPERIMENTAL SECTION

Materials. Commercially available reagents were used as received. 1,10-Phenanthroline-5,6-dione, 4,5-dibromo-*o*-phenylenediamine, dppzBr,[17] dppzBr$_2$, and [Re(CO)$_3$(dppzBr)Cl][17] were synthesized according to literature procedures, and analytical data found was identical to literature results. Dppz and ppp ligands were synthesized using the Schiff base condensation of 1,10-phenanthroline-5,6-dione with the appropriate diamine compound. [Re(CO)$_3$(L)Cl] compounds were produced by refluxing molar equivalents of Re(CO)$_5$Cl with the appropriate ligand in ethanol under a nitrogen atmosphere overnight. The cooled reaction mixture was filtered to obtain a yellow or orange solid. [Re(CO)$_3$(L)(py)]PF$_6$ compounds were synthesized by refluxing the corresponding [Re(CO)$_3$(L)Cl] compound with 1 equiv of AgOTf in MeCN under nitrogen overnight. The reaction mixture was filtered through Celite to remove AgCl, saturated NH_4PF_6(aq) was added, and acetonitrile was removed under reduced pressure. The solid was filtered and washed with distilled water. The resulting [Re(CO)$_3$(L)(CH$_3$CN)]PF$_6$ compound was refluxed with a 20× excess of pyridine in THF to give the [Re(CO)$_3$(L)(py)]PF$_6$ complex.[18]

11-Bromopyrido[2′,3′:5,6]pyrazino[2,3-f][1,10]phenanthroline (pppBr). Phendione (0.314 g, 1.49 × 10^{-3} mol) and 0.341 g of 2,3-diamino,5-bromopyridine were refluxed in 150 mL of ethanol for 12 h. The reaction mixture was cooled, and the cream solid was filtered. Yield = 0.3787 g (1.05 × 10^{-3} mol), 70%. ^{1}H NMR (400 MHz, $CDCl_3$): δ 9.736 (dd, 1H, J = 8 Hz, J = 1.6 Hz), 9.568 (dd, 1H, J = 8 Hz, J = 1.6 Hz), 9.352 (d, 1H, J = 2.4 Hz), 9.323 (dd, 2H, J = 4.4 Hz, 1.6 Hz), 8.907 (d, 1H, J = 2.4 Hz) 7.8374 (m, 2H). Anal. Calcd for $C_{17}H_8N_5Br$: C, 56.37; H, 2.23; N, 19.34. Found: C, 56.40; H, 2.11; N, 19.45. m/z (ESI POS): 383.98 {pppBr + Na$^+$}.

13-Bromo-11-trimethyldipyrido[3,2-a:2′,3′-c]phenazine (dppzBr-(CF$_3$)). Phendione (0.3 g, 1.427 × 10^{-3} mol) and 1.2 equiv of 3-bromo-4,5-diaminobenzotrifluoride (0.433 g, 1.713 × 10^{-3} M) were refluxed in 150 mL of ethanol for 8 h. The resulting solution was reduced to half the volume by rotary evaporation and was refrigerated for 1 h. The resulting cream solid was filtered and air-dried. Yield = 0.553 g (1.28 × 10^{-3} mol), 89%. ^{1}H NMR (400 MHz, $CDCl_3$): δ 9.717 (dd, 1H, J = 8.4 Hz, J = 2 Hz), 9.59 (dd, 1H, J = 8 Hz, J = 1.6 Hz), 9.325 (m, 2H), 8.651 (m, 1H), 8.392 (d, 1H, J = 2 Hz) 7.845 (m, 2H). Anal. Calcd for $C_{19}H_8N_4F_3Br{\cdot}2H_2O$: C, 49.05; H, 2.60; N, 12.05. Found: C, 49.39; H, 2.29; N, 12.09. m/z (ESI POS): 452.19 {dppzBr(CF3) + Na$^+$}.

fac-Chlorotricarbonyl (11-Bromopyrido[2′,3′:5,6]pyrazino[2,3-f][1,10]phenanthroline)rhenium ([Re(CO)$_3$(pppBr)Cl]). pppBr (0.2 g, 5.52 × 10^{-4} mol) and 0.2 g of Re(CO)$_5$Cl were refluxed in 100 mL of ethanol under a nitrogen atmosphere overnight. The resulting orange mixture was kept in the freezer for 4 h, and the orange solid was filtered and air-dried. Yield = 0.354 g (5.29 × 10^{-4} mol), 96%. ^{1}H NMR (400 MHz, $CDCl_3$): δ 9.942 (dd, 1H, J = 8 Hz, J = 1.2 Hz), 9.788 (dd, 1H, J = 8 Hz, J = 1.6 Hz) 9.515 (m 2H) 9.479 (d, 1H, J = 2.4 Hz) 9.006 (d, 1H, 2.4 Hz), 8.070 (dd, 2H). Anal. Calcd for $C_{20}H_8N_5O_3BrReCl{\cdot}0.5CH_3CH_2OH$: C, 36.51; H, 1.60; N, 10.41. Found: C, 36.53; H, 1.31; N, 10.53. m/z (ESI POS): 689.89 {[Re(CO)$_3$(pppBr)Cl] + Na$^+$)}.

fac-Chlorotricarbonyl (13-Bromo-11-trimethyldipyrido[3,2-a:2′,3′-c]phenazine)rhenium ([Re(CO)$_3$(dppzBr(CF$_3$))Cl]). dppzBr-(CF$_3$) (0.3 g, 6.94 × 10^{-4} mol) and 0.25 g of Re(CO)$_5$Cl (1 equiv) were refluxed in 125 mL of ethanol under a N_2 atmosphere overnight. The resulting orange solution was kept in the freezer for 1 h, and the orange solid was then filtered and air-dried. Yield = 0.469 g (6.38 × 10^{-4} mol), 92%. ^{1}H NMR (400 MHz, $CDCl_3$): δ 9.932 (dd, 1H, J = 8.4 Hz, J = 1.6 Hz) 9.819 (dd, 1H, J = 8.4 Hz, J = 1.6 Hz) 9.52 (m 2H) 8.743 (m, 1H), 8.51 (d, 1H, J = 1.6 Hz) 8.087 (m, 2H). Anal. Calcd for $C_{22}H_8N_4O_3F_3BrReCl$: C, 35.96; H, 1.10, 7.63. Found: C, 35.80; H, 1.48, N, 7.51. m/z (ESI POS): 756.89 {[Re(CO)$_3$(dppzBr(CF$_3$))Cl] + Na$^+$)} .

fac-Chlorotricarbonyl (11,12-Dibromodipyrido[3,2-a:2′,3′-c]-phenazine)rhenium ([Re(CO)$_3$(dppzBr$_2$)Cl]). dppzBr$_2$ ligand (0.2 g, 4.50 × 10^{-4} mol) and 0.162 g of Re(CO)$_5$Cl were refluxed in 100 mL of ethanol under a nitrogen atmosphere overnight. The cooled reaction mixture was filtered, and the yellow solid was filtered. Yield = 0.314 g (4.21 × 10^{-4} mol), 94%. ^{1}H NMR (400 MHz, $CDCl_3$): δ 9.783 (dd, 2H, J = 8 Hz J = 1.2 Hz) 9.482 (dd, 2H, J = 5.2 Hz, J = 1.6 Hz) 8.796 (s, 2H) 8.036 (dd, J = 8 Hz, J = 4.8 Hz). Anal. Calcd for $C_{21}H_8N_4O_3Br_2ClRe{\cdot}0.75C_2H_5OH$: C, 34.63; H, 1.61; N, 7.18. Found: C, 34.94; H, 1.35; N, 7.46. m/z (ESI POS): 768.81 {[Re-(CO)$_3$(dppzBr$_2$)Cl] + Na$^+$)}.

fac-Tricarbonyl (11-Bromopyrido[2′,3′:5,6]pyrazino[2,3-f][1,10]-phenanthroline)(pyridine)rhenium Hexafluorophosphate ([Re(CO)$_3$(pppBr)(py)]PF$_6$)·H$_2$O. [Re(pppBr)(CO)$_3$(CH$_3$CN)]PF$_6$ (0.215 g, 2.53 × 10^{-4} mol) and a 20× excess of pyridine (5.05 × 10^{-3} mol,

dx.doi.org/10.1021/ic403056g | Inorg. Chem. 2014, 53, 3126−3140

0.4 mL) were refluxed in 80 mL of THF under a nitrogen atmosphere for 4 h. The precipitate which had formed was hot filtered to give a gray solid. The gray solid was suspended in a small volume of acetonitrile (~20 mL) and filtered through Celite to remove unwanted side products giving a yellow solution. To this solution was added 10 mL of saturated aqueous NH_4PF_6, and the acetonitrile was removed under reduced pressure to give a yellow solid which was filtered and washed with water. Yield = 0.181 g (2.11×10^{-4} mol), 84%. ^{1}H NMR (400 MHz, $(CD_3)_2CO$): δ 10.1 (m, 4H), 9.55 (d, 1H, J =2.4), 9.16 (d, 1H, J = 2.4), 8.71 (m, 2H, pyridyl), 8.55 (m, 2H), 7.93 (m, 1H, pyridyl), 7.41 (m, 2H, pyridyl). Anal. Calcd for $C_{25}H_{13}N_6O_3BrRePF_6 \cdot H_2O$: C, 34.34; H, 1.73; N, 9.61. Found: C, 34.04; H, 1.66; N, 9.46. m/z (ESI POS): 710.98 $\{[Re(CO)_3(pppBr)(C_5H_5N)]^+\}$.

fac-Tricarbonyl (13-Bromo-11-trimethyldipyrido[3,2-a:2′,3′-c]-phenazine)(pyridine)rhenium Hexafluorophosphate ([Re(CO)$_3$(dppz Br(CF$_3$))(py)]PF$_6$)·H$_2$O. $[Re(dppzBr(CF_3))(CO)_3(CH_3CN)]PF_6$ (0.261 g, 3.19×10^{-4} mol) and a 20× excess of pyridine (6.39×10^{-3} mol, 0.514 mL) were refluxed in 30 mL of THF for 2 h, in which time the solution went from yellow to a dark orange. To the cooled solution was added 10 mL of saturated aqueous NH_4PF_6, and the THF was removed under reduced pressure to give a yellow solid which was filtered and washed with water. Yield = 0.208 g (2.22×10^{-4} mol), 70%. ^{1}H NMR (400 MHz, $(CD_3)_2CO$): δ 10.1 (m, 4H), 8.87 (s, 1H), 8.73 (m, 3H), 8.58 (m, 2H), 7.93 (m, 1H, pyridyl), 7.42 (m, 2H, pyridyl). Anal. Calcd for $C_{27}H_{13}N_5O_3BrPF_9Re \cdot H_2O$: C, 35.27; H, 1.59; N, 7.35. Found: C, 35.35; H, 1.56; N, 7.42. m/z (ESI POS): 777.97 $\{[Re(CO)_3(dppz\ Br(CF_3))(C_5H_5N)]^+\}$, 716.94 $\{[Re(CO)_3(dppzBr(CF_3)]^+ + H_2O\}$.

fac-Tricarbonyl (11,12-Dibromodipyrido[3,2-a:2′,3′-c]-phenazine)(pyridine)rhenium Hexafluorophosphate ([Re(CO)$_3$(dppzBr$_2$)(py)]PF$_6$). $[Re(dppzBr_2)(CO)_3(CH_3CN)]PF_6$ (0.15 g, 1.68×10^{-4} mol) and a 10× excess of pyridine (1.68×10^{-3} mol, 0.135 mL) were refluxed in 100 mL of THF for 4 h. The volume of the solution was then reduced under vacuum to about 30 mL and refrigerated overnight. The resulting precipitate was filtered and washed with water. Yield = 0.12 g (1.25×10^{-4} mol), 75%. ^{1}H NMR (400 MHz, $(CD_3)_2CO$): δ 10.01 (m, 4H), 8.89 (s, 1H), 8.71 (m, 2H, pyridyl), 8.53 (m, 2H), 7.93 (m, 1H, pyridyl), 7.4 (m, 2H, pyridyl). Anal. Calcd for $C_{28}H_{13}N_5O_3Br_2RePF_6$: C, 35.09; H, 1.37; N, 7.31. Found: C, 35.31; H, 1.55; N, 7.25. m/z (ESI POS): 813.41 $\{[Re(CO)_3(dppzBr_2)(C_5H_5N)]^+\}$.

fac-Tricarbonyl (11-Bromodipyrido[3,2-a:2′,3′-c]phenazine)-(pyridine)rhenium Hexafluorophosphate ([Re(CO)$_3$(dppzBr)(py)]-PF$_6$). $[Re(dppzBr)(CO)_3(CH_3CN)]PF_6$ (0.288 g, 3.52×10^{-4} mol) and a 20× excess of pyridine (7.04×10^{-3} mol, 0.567 mL) were refluxed in 50 mL of THF under a nitrogen atmosphere for 90 min, after which time a precipitate had formed. The reaction mixture was cooled to room temperature and the precipitate filtered to obtain an analytically pure solid. Yield = 0.220 g (2.57×10^{-4} mol), 73%. ^{1}H NMR (400 MHz, $(CD_3)_2CO$): δ 10.05−9.99 (m, 4H), 8.704 (m, 3H, pyridyl, dppz), 8.53 (m, 2H), 8.44 (d, 1H, J = 9.2 Hz), 8.29 (dd, 1H, J = 9.2 Hz, 2 Hz), 7.93 (m, 1H), 7.41 (m, 2H, py). Anal. Calcd for $C_{26}H_{14}N_5O_3BrRePF_6$: C, 36.50; H, 1.65; N, 8.19. Found: C, 36.55; H, 1.62; N, 8.09. m/z (ESI POS): 709.98 $\{[Re(CO)_3(dppzBr)(C_5H_5N)]^+\}$.

Physical Measurements. Spectroscopic-grade solvents (Sigma-Aldrich) were used for all spectroscopic measurements. Spectra were processed using GRAMS AI v8.00 (Thermo Scientific) and OriginPro v8.0 (OriginLab Corp.) software. Reduction potentials were measured against decamethylferrocenium/decamethylferrocene ($DMFc^+$/DMFc) on dichloromethane solutions, typically 1×10^{-3} M, with 0.1 M tetrabutylammonium hexafluorophosphate as a supporting electrolyte. Electronic absorption spectra were recorded in dichloromethane at room temperature, with concentrations of typically 1×10^{-4} M, on a Perkin-Elmer Lambda 950 instrument. Emission spectra were recorded in dichloromethane at room temperature with concentrations of typically 1×10^{-4} M, following degassing with argon for 10 min, on a Perkin-Elmer LS50B luminescence spectrometer using WinLab v4.00 software.

FT-Raman spectra were recorded on powder samples at room temperature using a Bruker Equinox-55 interferometer with a FRA 106/5 Raman accessory. A Nd:YAG excitation source was used with 1064 nm excitation wavelength. Raman photons were detected with a D418T liquid nitrogen cooled Ge diode detector. Spectra were measured with typically 64 scans and 80 mW power, with spectral resolution of 4 cm^{-1} using the Bruker OPUS v5.5 software package. Resonance Raman spectra were recorded using a previously described setup[19−22] on dichloromethane solutions with concentrations of typically 1−5 mM. Excitation wavelengths 350.7, 356.4, 406.7, and 413.1 nm were provided by a krypton ion laser (Innova I-302, Coherent Inc.), 457.9 nm was provided by an argon ion laser (Innova Sabre, Coherent Inc.) and 444.3 nm by a solid state diode laser (CrystaLaser).

TR^2 spectra were recorded at room temperature on typically 1 mM dichloromethane solutions. Samples were pumped and probed at 355 nm using pulsed third-harmonic radiation from a Brilliant (Quantel) Nd:YAG laser, and data were collected using a PI-MAX intensified camera (Princeton Instruments). Transient absorption and emission spectra were recorded on dichloromethane solutions with concentrations typically 1×10^{-5} M, which were degassed under argon for 10 min prior to measurement. Transients were acquired using a LP920K TA system (Edinburgh Instruments), with excitation at 355 nm from pulsed third-harmonic radiation from a Brilliant (Quantel) Nd:YAG laser at 1 Hz, and a Xe900 450 W xenon arc lamp controlled by a xP920 pulser as the probe source in TA mode. Photons were dispersed using a TMS300-A Czerny-Turner monochromator with 1800 grooves mm^{-1} grating, recorded on a R928 (Hamamatsu) photomultiplier, and transcribed on a TDS3012C (Tektronix) digital oscilloscope. The change in optical density (ΔOD) is found from I_b/I_T in which I_b is the intensity of transmitted light before the excitation pulse and IT is the intensity of transmitted light after the excitation pulse.

TRIR spectroscopy was carried out at the University of Nottingham on an apparatus that has been described previously.[10,23] Briefly, the output from a commercial Ti:sapphire oscillator (MaiTai)/regenerative amplifier system (Spitfire Pro, Spectra Physics) is split and used to generate 400 nm pump pulses and a tunable mid-IR pulse with a spectral bandwidth of 180 cm^{-1} and a pulse energy of ca. 2 μJ at 2000 cm^{-1}. Half of the IR pulse is reflected onto a single-element mercury cadmium telluride (MCT) detector (Kolmar Technology) to serve as a reference, and the other half serves as the probe beam, which is focused and overlaps with the pump beam at the sample position. The 400 nm pump pulse is optically delayed (up to 3 ns) by a translation stage (LMA Actuator, Aerotech) and focused onto the sample with a quartz lens. The focus spot of the probe beam was adjusted to be slightly smaller than that of the pump beam in order to ensure that the area probed corresponds to excited molecules. The broad-band-transmitted probe pulse is detected with an MCT array detector (Infrared Associates), which consists of 128 elements (1 mm high and 0.25 mm wide). The array detector is mounted in the focal plane of a 250 mm IR spectrograph (DK240, Spectra Product) with a 150 grooves mm-1 grating, resulting in a spectral resolution of ca. 4 cm^{-1} at 2000 cm^{-1}. The signals from the array detector elements and the single-element detector are amplified with a 144-channel amplifier and digitized by a 16-bit analogue-to-digital converter (IR-0144, Infrared Systems Development Corp.). A Harrick flowing solution cell with 2 mm thick CaF_2 windows and a path length of 350 μm is mounted on a motorized cell mount that moves the cell rapidly in x and y dimensions throughout the experiment. Consequently, each laser pulse illuminates a different volume of the sample, reducing heating and degradation of the sample solution.

Computational Methods. Calculations were performed using the Gaussian09 package.[24] Geometry optimization and harmonic vibrational frequency calculations were performed in vacuo using density functional theory (DFT), employing the B3LYP functional. A LANL2DZ effective core potential and associated basis set was used for the rhenium atoms, while the 6-31G(d) basis set was used for all other atoms. Time-dependent density functional theory (TD-DFT) calculations using the B3LYP and CAM-B3LYP funtional were run both in vacuo and with a dichloromethane solvent field using the

dx.doi.org/10.1021/ic403056g | Inorg. Chem. 2014, 53, 3126−3140

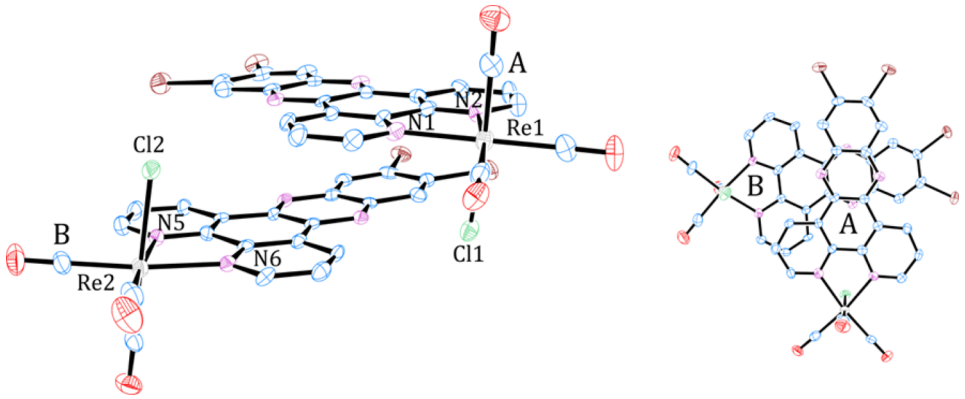

Figure 3. ORTEP views of the arrangement of $[Re(CO)_3(dppzBr_2)Cl]$ molecules (A and B) within the unit cell. Ellipsoid probabilities are at 50%.

keyword scrf (solvent = dichloromethane). The default self-consistent reaction field method is the polarizable continuum model (PCM) in Gaussian09. Calculated vibrational spectra were generated using Gaussum v2.2.5 software, and scaled to give the lowest value for the mean absolute deviation for band position from experimental data, with scale factors typically around 0.975. Raman activities calculated by G09 are converted to Raman scattering cross sections using an intensity correction.[25] Vibrational modes were illustrated using Molden.[26]

RESULTS AND DISCUSSION

Structure and Modeling. The structures of ligands and complexes were optimized using density functional theory (DFT) calculations, utilizing the B3LYP functional, the LANL2DZ basis set for rhenium, and the 6-31G(d) basis set for the remaining atoms. Since crystallographic data could not be obtained for many of these compounds, a comparison of modeled vibrational spectra and experimental spectra can provide a good method of validating these calculations.[3,10,15,27−30] Calculated structural data are as expected, with the dppz backbackbone planar for both ligands and complexes. In the rhenium(I) complexes, the Re(I) center sits slightly out of the plane of the dppz ligand, and this behavior is more pronounced for $[Re(CO)_3(L)Cl]$ complexes than $[Re(CO)_3(L)(py)]^+$. Crystal structures were obtained for complexes $[Re(CO)_3(dppzBr_2)Cl]$ and $[Re(CO)_3(dppzBr)(py)]PF_6$. The former crystallizes in the triclinic space group *P*-1, with two distinct molecules per unit cell. These two molecules are packed perpendicular to one another, via π stacking between parts of the dppz ligand, as can be seen in Figure 3. The centroid-to-centroid distance is 3.3 Å long. The bond lengths are very similar between the two molecules and also correspond well to calculated values, as shown in Table 1.

$[Re(CO)_3(dppzBr)(py)]PF_6$ crystallizes in the monoclinic space group $P2_{1/n}$, with four complex molecules and four PF_6^- anions in the unit cell. As shown in Figure 4, the dppz ligand is disordered over two sites, i.e., the superposition of the two enantiomers due to the relative position of the bromine atom. The disorder of the dppzBr ligand was modeled with 80/20% occupancy, the moiety including the bromine atom labeled Br1 is the major component, and these atoms are modeled with anisotropic displacement parameters. The 20% component (moiety including Br_2) is well behaved, and the atoms are modeled isotropically. The crystal structure of the related complex, $[Re(dppzBr)(CO)_3Cl]$, was published by Lundin et al.[17] where the bromine atoms are disordered over the two sites with 50:50 occupancy, consistent with the presence of two enantiomers in equal amounts. However, the dppzBr ligand moiety was not disordered. The distribution of enantiomers in the $[Re(dppzBr)(CO)_3(py)]PF_6$ complex presented here is most probably 50:50, as observed in the related complex published by Lundin et al.[17] The 80/20 occupancy of the dppzBr ligand is used to resolve the disorder of the structure as a crystallographic necessity, and is not intended to imply a resolution of enantiomers. Bond lengths and angles correspond reasonably with calculated values, shown in Table 2.

Table 1. Important Bond Lengths (Å) and Angles (deg) for $[Re(CO)_3(dppzBr_2)Cl]$

Experimental				Calculated	
Re(1)−N(1)	2.171	Re(2)−N(5)	2.173	Re−N(a)	2.210
Re(1)−N(2)	2.180	Re(2)−N(6)	2.182	Re−N(b)	2.210
Re(1)−Cl(1)	2.469	Re(2)−Cl(2)	2.471	Re−Cl	2.518
N(1)−Re(1)−N(2)	75.7	N(5)−Re(2)−N(6)	75.3	N(a)−Re-N(b)	74.8

Ground-State Vibrational Spectroscopy. In the absence of crystallographic data, calculated and experimental Raman spectra may be compared in order to validate calculations,[10,15,21,25,31,32] as shown in Figure 5 for $dppzBr_2$. The correlation between spectra is quantified using the mean absolute deviation (MAD) between the position of calculated and experimental bands with a relative intensity of at least 20% of that of the most intense band, in the range 1000−1600 cm^{-1}. Carbonyl bands are observed generally in the range 1900−2100 cm^{-1} but usually have low intensity in nonresonant spectra for this compound type. These are not included in MAD calculations because their frequencies are not well predicted by calculations due to significant anharmonicity which is difficult to model and would require different scaling. A scale factor is used to adjust calculated spectra which minimizes the MAD;[21,33,34] scale factors and MADs are shown in Table S1 (Supporting Information). MAD values range from 4.3 to 9.0 cm^{-1}; as these are all relatively low (less than 10 cm^{-1}), the calculations are considered to model compounds well.[35]

FT-Raman bands, calculated frequency, vibrational mode, and assignments are shown in Table 3, Figures S1−S6 and Tables S2−S4 (Supporting Information) for ligands and metal complexes. These data are useful in establishing whether phen and phz modes can be distinguished and, if so, used to identify where MLCT-type transitions terminate. All ligands and complexes show the typical 1400 cm^{-1} band for dppz-based systems; this is assigned as a vibration of the phenazine section of the ligand.[3,10,15] The ligands all display bands around 1034

dx.doi.org/10.1021/ic403056g | Inorg. Chem. 2014, 53, 3126−3140

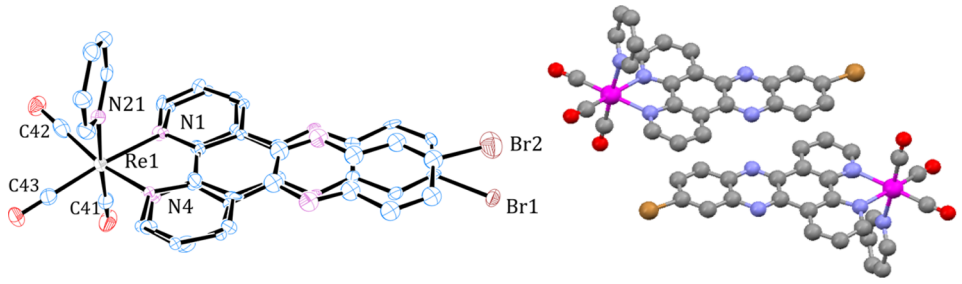

Figure 4. ORTEP diagram of $[Re(CO)_3(dppzBr)(py)]PF_6$ (ellipsoids at 50% probability level; H, atoms and PF_6 anion not shown). Packing arrangement with ligand atoms corresponding to 80% occupancy moiety shown.

Table 2. Important Bond Lengths (Å) and Angles (deg) for $[Re(CO)_3(dppzBr)(py)]PF_6$

Experimental				Calculated	
Re(1)–N(1)	2.154	Re(1)–C(42)	1.900	Re–N(1)	2.215
Re(1)–N(4)	2.189	Re(1)–C(43)	1.928	Re–N(4)	2.215
Re(1)–N(21)	2.205	Re(1)–C(41)	1.938	Re–N(21)	2.275
N(1)–Re(1)–N(4)	75.7			N(1)–Re-N(4)	75.0

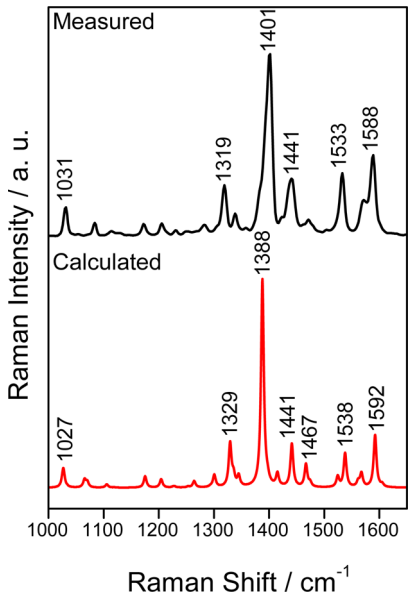

Figure 5. Comparison of measured (black) and calculated (red, B_3LYP, in vacuo) FT-Raman spectra for $dppzBr_2$.

cm^{-1} due to delocalized modes and bands around 1585 cm^{-1} attributed to phenanthroline modes. Complexes consistently show bands around 1055 cm^{-1}, which vary a little in the extent of localization to the phen part; all show phen modes around 1320 cm^{-1}, delocalized dppz modes around 1450 cm^{-1} and 1600 cm^{-1} modes due to phen vibrations. $[Re(CO)_3(L)(py)]^+$ complexes all have pyridine ring breathing modes at 1017 cm^{-1}.

Electrochemical Studies. The first reduction potentials of ligands, $[Re(CO)_3(L)\ Cl]$ and $[Re(CO)_3(L)(py)]^+$ complexes are shown in Table 4; ligands and complexes all show oxidation as an irreversible wave toward the limit of the solvent window and, hence, are not reported.

Because the LUMO of dppz-based compounds is localized to the phenazine section, which is where these compounds are substituted, the change in reduction potential indicates how the energy of the phz MO is altered by the substituent, with the order of ligand reduction potentials reflecting the relative electron-withdrawing nature. As can be seen in Table 4, $dppzBr(CF_3)$ and pppBr have the most positive reduction potentials; therefore, the LUMO is most affected by these electron-withdrawing substituents. Coordination of $\{Re(CO)_3Cl\}$ shifts reduction potentials 240–290 mV more positive, which indicates that the Re center significantly affects the phz MO; this is comparable to other Re(I) compounds.[10,17,28] The chloride ligand is a π-donor, and hence, the π backbonding from Re to dppz is stronger when the ancillary ligand is Cl^- than pyridine. When coordinated to $\{Re(CO)_3(py)\}^+$, the reduction potentials shift 100–120 mV more positive relative to the ligand. Cyclic voltammograms are shown for $dppzBr(CF_3)$ and its two complexes in Figure 6. In addition to lowering the energy of the LUMO relative to the corresponding Cl complex, pyridine lowers the energy of the dπ orbitals also; see Figure 7.

Electronic Absorption Spectra and TD-DFT Calculations. Electronic absorption spectra of ligands and complexes are shown in Figure 8. These do not differ significantly from unsubstituted dppz and its complexes,[1,38,39] and therefore, transitions are likely to be similar in nature. The ordering of the lowest lying unoccupied molecular orbitals is the same for all ligands as for unsubstituted dppz, and likewise, the complexes are the same as for $[Re(CO)_3(dppz)Cl]$; the difference between ligand and complex is that the b_1(phen) MO is higher in energy than the delocalized a_2 MO in the ligand but lower in the complex. However, the extent of mixing between phen and phz MOs is greater, which is especially obvious for $[Re(CO)_3(dppzBr_2)(py)]PF_6$ L+1.

Experimental electronic absorption data and TD-DFT predicted transitions are given in Table 6. The transitions listed were predicted using the CAM-B3LYP functional because this tends to give more accurate energy values the B3LYP for charge-transfer transitions, which occur here. Although TD-DFT calculations tend to offset absolute energy, these cannot be scaled because the magnitude of the error is strongly dependent on the nature of the transition.[40] However, they tend to give reasonable values for energy differences, and are qualitatively reliable with respect to the nature of transitions and the ordering of these. The blue-shift of the tailing shoulder when Cl is replaced with pyridine is correctly predicted. Pyridine lowers the energy of the unoccupied molecular orbitals relative to the equivalent Cl complex, but also lowers the energy of the dπ orbitals, and this effect is greater; therefore, the energy gap is larger.

Essentially, all ligands are predicted to show $\pi \rightarrow \pi^*$ electronic transitions, while complexes are predicted to show π

dx.doi.org/10.1021/ic403056g | Inorg. Chem. 2014, 53, 3126–3140

Table 3. Band Assignments for Selected Vibrational Modes of Ligands and Complexes Calculated at the B3LYP/6-31G(d) Level

Compound	phen	phen	phz	phz	delocalized	phz	phen	phz	phen
dppz		1316		1406			1450	1545	
$dppzBr_2$	1031	1319		1401		1441		1533	1588
dppzBr	1031	1326		1403			1431	1535	1586
$dppzBr(CF_3)$	1036	1329		1401			1449	1540	1587
pppBr	1034			1391				1538	1584
$[Re(CO)_3(dppzBr_2)Cl]$	1055	1317		1397	1451			1542	1598
$[Re(CO)_3(dppzBr)Cl]$	1055	1321		1406	1451				1599
$[Re(CO)_3(dppzBr(CF_3))Cl]$	1056	1324	1361	1399	1451				1596
$[Re(CO)_3(pppBr)Cl]$	1054	1324		1390			1452	1488	1598
$[Re(CO)_3(dppzBr_2)(py)]^+$	1055	1317		1394	1447				1596
$[Re(CO)_3(dppzBr)(py)]^+$	1055	1317		1404	1447				1596
$[Re(CO)_3(dppzBr(CF_3))(py)]^+$	1056	1322	1361	1403	1449				1595
$[Re(CO)_3(pppBr)(py)]^+$	1054	1325		1391	1450				1598

Table 4. Electrochemical Data for All Ligands and Complexes[a,b]

Compound	E_{red}[a] (V vs SCE)	ΔR[b] (V)
dppzBr	−1.11	
$dppzBr_2$	−1.08	
$dppzBr(CF_3)$	−0.95	
pppBr	−0.93	
$[Re(CO)_3(dppzBr)Cl]$	−0.87	0.24
$[Re(CO)_3(dppzBr_2)Cl]$	−0.79	0.29
$[Re(CO)_3(dppzBr(CF_3))Cl]$	−0.68	0.27
$[Re(CO)_3(pppBr)Cl]$	−0.67	0.26
$[Re(CO)_3(dppzBr)(py)]PF_6$	−0.76	0.11
$[Re(CO)_3(dppzBr_2)(py)]PF_6$	−0.67	0.12
$[Re(CO)_3(dppzBr(CF_3))(py)]PF_6$	−0.58	0.10
$[Re(CO)_3(pppBr)(py)]PF_6$	−0.56	0.11

[a]Reduction potentials are recorded in CH_2Cl_2 against $DMFc^+$/DMFc with Ag/AgCl reference electrode and converted to SCE with −0.045 V.[36,37] Irreversible oxidation potentials were observed toward the solvent limit. [b]The change in reduction potential upon coordination for the $\{Re(CO)_3Cl\}$ complexes and change in reduction potential upon coordination of pyridine ligand compared to $\{Re(CO)_3Cl\}$ complexes.

→ π* transitions, MLCT to phen and MLCT to phz transitions. Absorption spectra for ligands are consistent with π → π* transitions, similar to those observed for other substituted dppz systems.[3,4,28,41] Experimentally, these start at approximately 400 nm. Complexes also exhibit transitions around 350−400 nm, although these are shifted relative to the free ligand due to metal binding, consistent with these being ligand-centered π → π* type also. Complexes show tailing shoulders on these bands, extending out to around 500 nm. Previous studies on dppz systems, in addition to TD-DFT calculations and resonance Raman spectroscopy, suggest that this shoulder is due to MLCT transitions.[4,41] It is possible to correlate the electrochemical and electronic absorption data in that the MLCT transition corresponds to the ΔE ($E_{red} - E_{ox}$).[42] However, in this case some caution is needed as the orbitals involved in reduction need not necessarily be major contributors to the optical transitions. In this case, the predominant acceptor MOs in the observed MLCT transitions are phen-based (see Table 5, L+1). However, the MO at which reduction occurs is phz-based (see Table 5, LUMO). The electrochemical data show a stabilization of the phz-based redox MO upon py substitution; however the MLCT transition is blue-shifted (see Figure 8) as is typical for Re(L) compounds.[43]

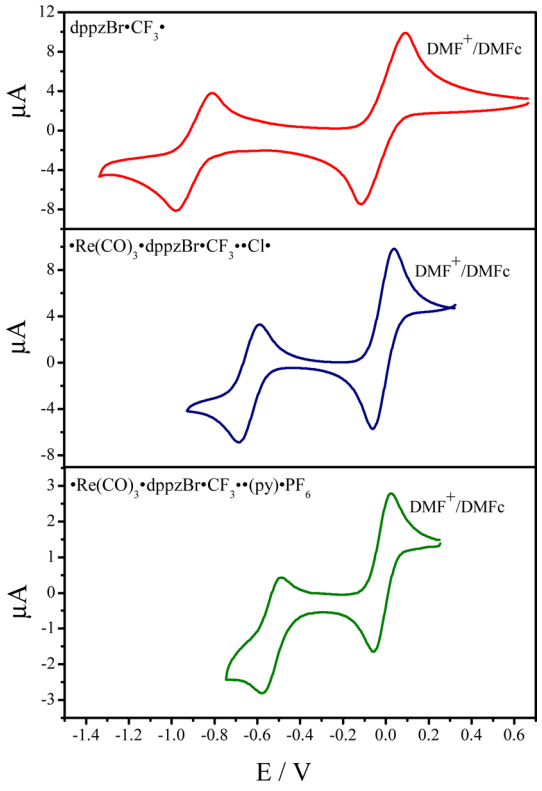

Figure 6. Cyclic voltammograms for the first reduction process of $dppzBr(CF_3)$, $[Re(CO)_3(dppzBr(CF_3))Cl]$, and $[Re(CO)_3(dppzBr(CF_3))(py)]PF_6$, measured in CH_2Cl_2 against Ag/AgCl reference electrode with scanning speed 100 mVs^{-1}. The peak at 0 V in all CVs is due to $DMFc^+$/DMFc and is labeled as such.

These two experiments are consistent with DFT calculations which show that the phz MO is stabilized by py substitution (Figure 7) but the HOMO−LUMO energy gap increases. TD-DFT calculations show low energy optical transitions with significant phen (L+1) character, Table 6.

Resonance Raman Spectroscopy. The nature of electronic transitions can be probed using resonance Raman spectroscopy, as when the excitation wavelength coincides with an electronic transition the resonance effect causes significant enhancement of vibrational modes which involve the active chromophore.[44,45] Consequently, analysis of the pattern of band enhancements at a given wavelength is informative on the nature of the transition. MLCT transitions can be characterized

dx.doi.org/10.1021/ic403056g | Inorg. Chem. 2014, 53, 3126−3140

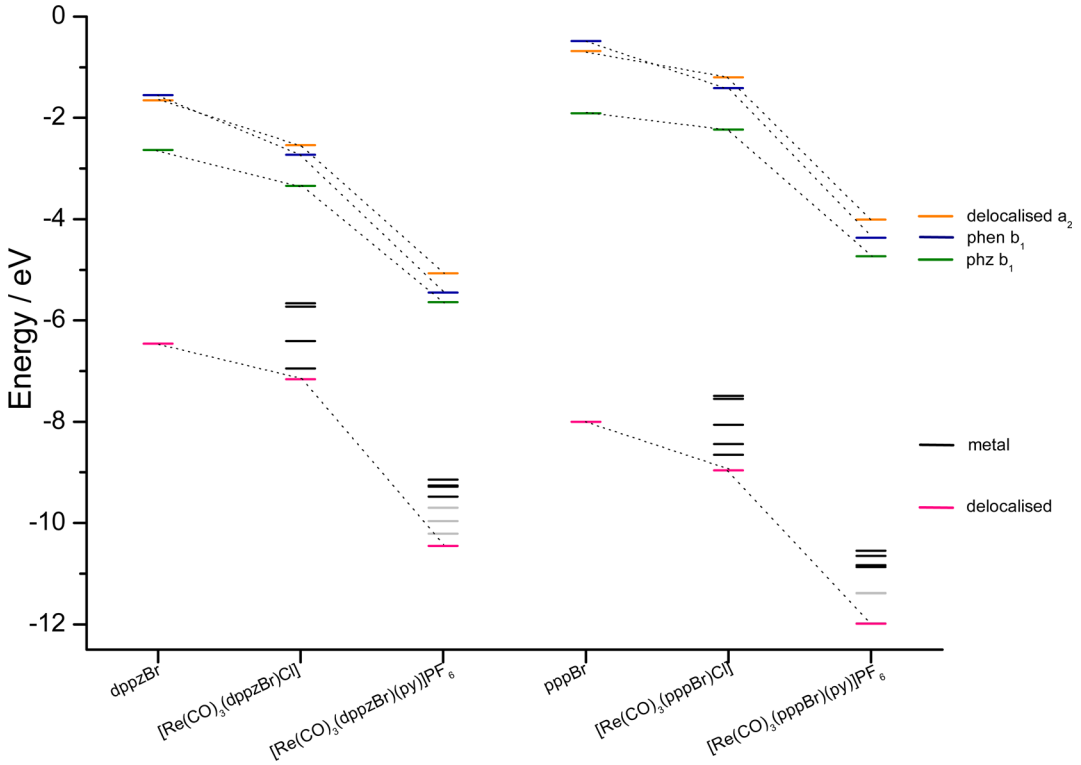

Figure 7. Molecular orbital energy of selected compounds showing the effect of the metal and ancillary ligands. MO energy is from optimized structures calculated using the B3LYP functional, dichloromethane solvent field implemented with the PCM model.

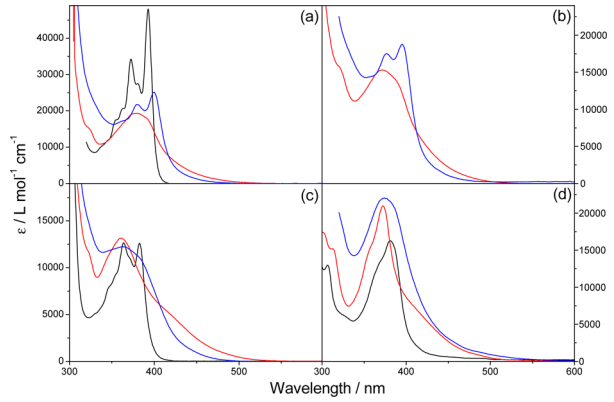

Figure 8. UV−vis absorption spectra of ligands (shown in black); $[Re(CO)_3(L)Cl]$ complexes (red) and $[Re(CO)_3(L)(py)]PF_6$ complexes (blue) for the $dppzBr_2$ (a), dppzBr (b), $dppzBr(CF_3)$ (c), and pppBr (d) sets.

by enhancement of the symmetric stretch of the carbonyl groups because in such states the metal center is oxidized, reducing the extent of π-backbonding, and thus, these bonds change in length.[25] Resonance Raman studies therefore support the assignment of MLCT transitions, as carbonyl bands show intensity enhancement at wavelengths longer than 406 nm. It is difficult to specify at which wavelength the MLCT transition is in electronic absorption spectra, as it appears as a shoulder. Ligands were too emissive to measure, as any spectral bands were obscured by this fluorescence. The normal (nonresonant) Raman spectrum of $[Re(CO)_3(dppzBr_2)Cl]$ is dominated by a band at 1399 cm^{-1}, assigned by DFT calculations and by comparison to previous dppz studies as a phenazine band. The UV wavelengths (350.7 and 356.4 nm) show enhancement of a 1537 cm^{-1} phenazine mode relative to FT Raman spectrum, consistent with the dominant chromophore being $\pi \rightarrow \pi^*$(phz). As the excitation wavelength is tuned toward longer wavelengths, this band is diminished, while delocalized modes (1314, 1485 cm^{-1}) and a phenanthroline mode (1597 cm^{-1}) show greater relative enhancement. The symmetric stretch of carbonyl groups (2025 cm^{-1}) also shows enhancement with 406.7, 413.1, and 444.3 nm excitation, which is indicative of a MLCT state. This is consistent with previous studies and with TD-DFT calculations. However, because the pattern of band enhancement for the ligand vibrational modes at 406.7 and 413.1 nm is different from that at 444.3 and 457.9 nm (see Figure 9), there may be a shift from MLCT to phz/phen at shorter wavelengths to MLCT(phen) at longer wavelengths.

The nonresonant spectrum of $[Re(CO)_3(dppzBr_2)(py)]^+$ is similar to that of the Cl complex; similar patterns of bands are also observed in resonance Raman spectra with a phz mode (1547 cm^{-1}) enhanced in the UV region (likely $\pi \rightarrow \pi^*$(phz)) and delocalized phen and carbonyl modes (1485, 1312, and 2039 cm^{-1}, respectively) enhanced in the visible, indicative of a MLCT state, which may populate a phen MO. As may be expected, the normal Raman spectrum of $[Re(CO)_3(pppBr)Cl]$ is dominated by the phenazine mode (1390 cm^{-1}); despite the extra nitrogen, this is not altered significantly, and in fact, the shift in the vibrational mode frequency is overestimated by DFT. Resonant spectra at UV wavelengths show only this mode and a 1451 cm^{-1} delocalized dppz mode with any significant intensity, consistent with a ligand-centered $\pi \rightarrow \pi^*$(phz) state. Wavelengths at 406.7−457.9 nm show the enhancement of bands in the region 1570−1600 cm^{-1} attributed to both phen and phz modes, as well as the carbonyl symmetric stretch at 2027 cm^{-1}, consistent with a MLCT state. Resonance Raman spectra for $[Re(CO)_3(pppBr)(py)]^+$ in-

dx.doi.org/10.1021/ic403056g | Inorg. Chem. 2014, 53, 3126−3140

Table 5. Molecular Orbitals Calculated with TD-DFT To Be Involved in Significant Electronic Transitions, Calculated Using CAM-B3LYP Functional in Dichloromethane Solvent Field Implementing the PCM Model

Compound	LUMO	L+1	L+2
pppBr	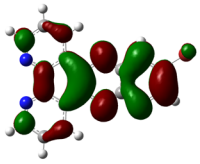	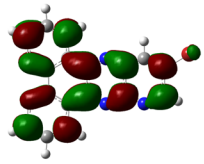	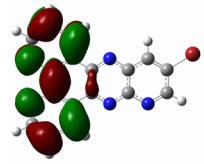
$dppzBr_2$	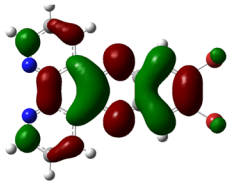	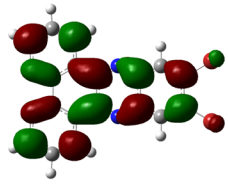	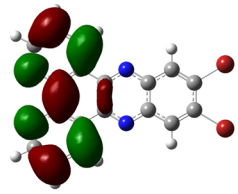
$[Re(CO)_3(dppzBr_2)Cl]$	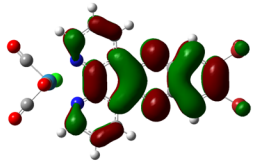	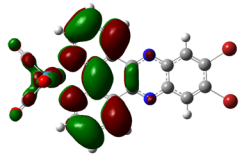	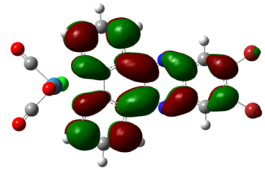
$[Re(CO)_3(dppzBr_2)(py)]PF_6$	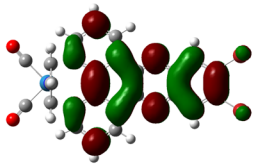	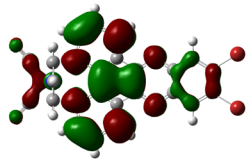	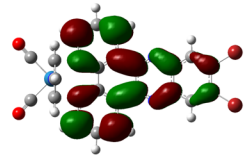

dicate the natures of transitions are very similar. $[Re(CO)_3(dppzBr(CF_3))Cl]$ shows enhancement of resonance Raman bands at 1345 and 1549 cm^{-1} with UV excitation (350.7 and 356.4 nm), which are both delocalized dppz modes, as a result of a $\pi \rightarrow \pi^*$ transition. In the visible region (406.7−457.9 nm), phen bands at 1493 and 1598 cm^{-1} show strong enhancement, in addition to a carbonyl band at 2027 cm^{-1}. This is consistent with MLCT to phen in this complex. $[Re(CO)_3(dppzBr(CF_3))(py)]^+$ shows a very similar pattern, with delocalized modes (1345, 1549 cm^{-1}) enhanced at UV wavelengths and phen (1494, 1597 cm^{-1}) and carbonyl (2029 cm^{-1}) modes enhanced in the visible, again consistent with a ligand-centered $\pi \rightarrow \pi^*$ transition at the shortest wavelengths and MLCT to phen at longer wavelengths. A $[Re(CO)_3(dppzBr)Cl]$ resonance Raman spectrum at 356.4 nm was published by Walsh et al.[32] and is consistent with recorded data. Spectra show that with 350.7 and 356.4 nm excitation a 1547 cm^{-1} phz band is enhanced, while in the visible bands are enhanced at 1490 cm^{-1} (phen), 1578 cm^{-1} (phen), and 2025 cm^{-1} (carbonyl symmetric stretch). The pyridine complex shows a similar pattern, with a 1538 cm^{-1} phz band enhanced in the UV, and delocalized dppz modes at 1316 and 1491 cm^{-1}, as well as the 2039 cm^{-1} carbonyl band, enhanced in the visible. This is again consistent with a ligand centered transition at short wavelengths, and a MLCT transition at longer wavelengths.

It appears that in some cases the "block" between the phen and phz parts of the molecule, which usually limits the oscillator strength of MLCT to phz type transitions, is broken, as both MLCT to phen and MLCT to phz are predicted with similar oscillator strengths. Resonance Raman studies may support the assertion that MLCT to phen and MLCT to phz transitions are both occurring, e.g., for the $dppzBr_2$ complexes. Many of the molecular orbitals in these compounds show extensive delocalization across the dppz ligand, in particular for $[Re(CO)_3(dppzBr_2)(py)]PF_6$, which has L+1 (phen in most compounds) which is extended over the whole dppz ligand. This interesting phz/phen mixing may be allowing MLCT phz transitions to gain intensity (Figure 10).

Emission and Lifetime Studies. Of compounds for which a signal was observed, all except $[Re(CO)_3(pppBr)(py)]^+$ show very short emission lifetimes at 298 K in CH_2Cl_2, decaying with the laser pulse. The lifetime values for the excited state(s) measured in transient absorption spectra (the absorbing state) are able to be measured as they are longer than the laser pulse. Values are shown in Table 7. For the three pairs of complexes for which the lifetime could be measured for both $\{Re(CO)_3Cl\}$ and $\{Re(CO)_3(py)\}$ compounds, the lifetime of the dark state is longer for the pyridine complex than the chloro complex. A potential explanation for this behavior is that an initially populated $^3\pi \rightarrow \pi^*$(phz) state, which is the measured dark state, may deactivate to a ^{3}MLCT state. We suggest that this ^{3}MLCT state is higher in energy than the $^3\pi \rightarrow \pi^*$(phz) state in the pyridine complexes, while in the chloro complexes this state is lower in energy than the $^3\pi,\pi^*$(phz) state. Consequently, the chloro complexes show rapid deactivation of the measured dark state by conversion to the MLCT state, while this does not occur in the pyridine complexes because the

dx.doi.org/10.1021/ic403056g | Inorg. Chem. 2014, 53, 3126−3140

Table 6. Experimental Absorption Data and CAM-B3LYP (Dichloromethane Solvent Field) TD-DFT Calculated Electronic Transitions for the Compounds Studied

	Experimental		Calculated			Mulliken charge density change (%)			
Compound	λ (nm)	ε (L mol^{-1} cm^{-1})	λ (nm)	f	major MO configurations (% contribution)	metal	phen	phz	substituent(s)
$dppzBr_2$	373	68520	264	0.501	H-3→L+2 (33),H→L+1 (30)		72→67 (−5)	21→33 (+12)	8→1 (−7)
	394	95094	333	0.591	H-1→L (90)		38→23 (−15)	50→75 (+25)	12→1 (−11)
pppBr	381	16260	335	0.570	H-1→L (47), H→L (45)		57→19 (−38)	37→81 (+44)	6→1 (−5)
$dppzBr(CF_3)$	364	12659	319	0.417	H-1→L (86)		45→23 (−22)	54→75 (+21)	2→2 (0)
	383	12590	326	0.045	H→L (96)		54→22 (−32)	39→76 (+37)	7→2 (−5)
dppzBr	329	7000							
	366	6100	351	0.213	H-2→L (83),H→L+1 (12)		48→25 (−23)	46→74 (+28)	6→1 (−5)
	385	6800	373	0.032	H→L (92)		48→21 (−27)	44→78 (+34)	8→1 (−7)
$[Re(CO)_3(dppzBr_2)Cl]$	381	16580	327	0.239	H-4→L (59), H-1→L+1 (27)	30→2 (−28)	23→61 (+38)	33→36 (+3)	14→1 (−13)
			350	0.358	H-1→L (42), H-1→L+1 (46)	76→3 (−73)	7→63 (+56)	15→32 (+17)	2→ (−1)
$[Re(CO)_3(dppzBr_2)\ (py)]PF_6$	381	29380	273	0.192	H-1→L+4 (50)	78→62 (−16)	11→23 (+12)	11→11 (0)	0→5 (+5)
	401	33920	336	0.690	H-4→L (32), H→L (42)	65→2 (−63)	11→40 (+29)	24→57 (+33)	1→0 (−1)
$[Re(CO)_3(pppBr)Cl]$	373	20990	328	0.222	H-3→L (49), H-1→L+1 (30)	35→2 (−33)	23→45 (+22)	31→52 (+21)	10→1 (−9)
			361	0.001	H→L (33), H→L+1 (64)	97→4 (−93)	3→67 (+64)	0→28 (+28)	0→0 (0)
$[Re(CO)_3(pppBr)(py)]PF_6$	373	22052	343	0.336	H→L (49), H→L+1 (35)	75→3 (−72)	10→58 (+48)	10→39 (+29)	5→1 (−4)
$[Re(CO)_3(dppzBr(CF_3))Cl]$	363	13090	351	0.227	H-1→L (43), H-1→L+1 (51)	59→3 (−56)	34→60 (+26)	7→32 (+25)	0→4 (+4)
$[Re(CO)_3(dppzBr(CF_3))(py)]PF_6$	363	12240	330	0.412	H-4→L (17), H→L (40), H→L+1 (34)	70→2 (−68)	13→51 (+38)	16→45 (+29)	1→1 (0)
			337	0.069	H-1→L (88), H-1→L+1 (10)	89→1 (−88)	9→43 (+34)	2→55 (+53)	0→2 (+2)
$[Re(CO)_0(dppzBr)Cl]$	372	15300	326	0.162	H-3→L (68), H-1→L+1 (15)	17→1 (−16)	21→40 (+19)	52→58 (+6)	11→0 (−10)
			346	0.309	H-1→L (38), H-1→L+1 (52)	87→4(−83)	7→61 (+54)	5→35 (+30)	1→0 (−1)
$[Re(CO)_3(dppzBr)(py)]PF_6$	376	17290	270	0.519	H-4→L+1 (31), H-2→L+2 (11), H-1→L+4(13)	32→17 (−14)	21→63 (+44)	27→41 (+14)	7→0 (−7)
	395	18610	333	0.500	H-2→L (30), H→L (45)	45→1 (−44)	15→42 (+27)	34→56 (+22)	7→1 (−6)

dx.doi.org/10.1021/ic403056g | Inorg. Chem. 2014, 53, 3126−3140

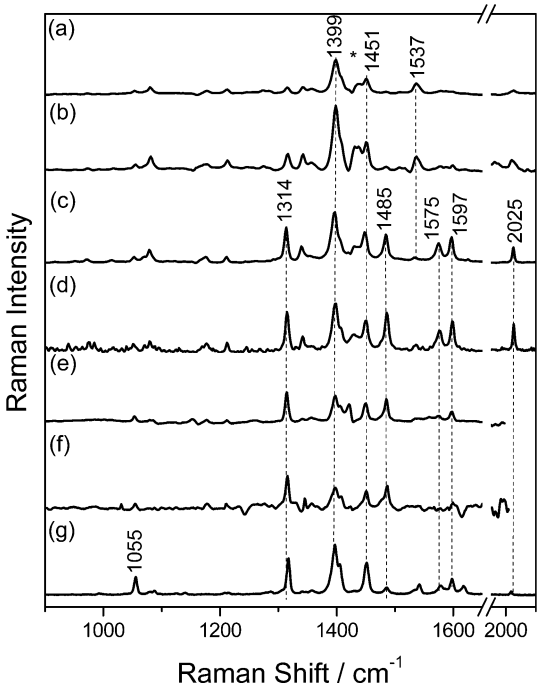

Figure 9. Resonance Raman spectra of $[Re(CO)_3(dppzBr_2)Cl]$ (0.1 mM DCM) at (a) 350.7 nm, (b) 356.4 nm, (c) 406.7 nm, (d) 413.1 nm, (e) 444.3 nm, (f) 457.9 nm, and (g) 1064 nm (in solid state). Solvent bands marked *.

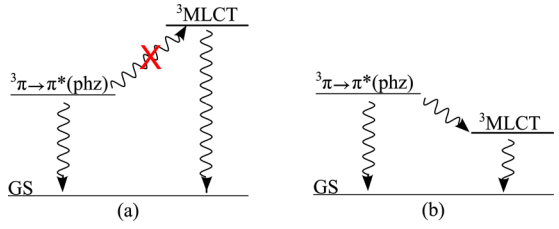

Figure 10. Simplified energy diagram for (a) $[Re(CO)_3(L)(py)]PF_6$ and (b) $[Re(CO)_3(L)Cl]$.

Table 7. Transient Absorption and Emission Lifetimes at 278 K in CH_2Cl_2

Compound	absorption τ (ns)	probe λ	emission τ (ns)	λ
$Re(CO)_3(dppzBr_2)Cl$	3200	550	<10	440
$[Re(CO)_3(dppzBr_2)(py)]^+$	6730	550	157	540
$Re(CO)_3(pppBr)Cl$	n.s.		<10	610
$[Re(CO)_3(pppBr)(py)]^+$	390, 6460	550	207	550
$Re(CO)_3(dppzBr(CF_3))Cl$	<10	650	<10	590
$[Re(CO)_3(dppzBr(CF_3))(py)]^+$	7880	550	<10	600
$Re(CO)_3(dppzBr)Cl$	<10	480	<10	600
$[Re(CO)_3(dppzBr)(py)]^+$	4500	490	n.s.	

^{3}MLCT state is higher energy. Such behavior is similar to that observed by Kuimova and co-workers,[46] where the complex $[Re(CO)_3(Cl)(dppzCl_2)]$ showed MLCT(phz) in time-resolved IR studies, and the py complex showed intraligand $\pi\pi^*$ (dppz). Lowering of the $^3\pi,\pi^*$ phz energy with py substitution is consistent with the electrochemical data that show stabilization of the π^* phz MO. Such an effect is not manifest in the UV spectra as the MLCT (Re → phen) dominates the more intense low energy transition ($^3\pi,\pi^*$ is formally spin forbidden and thus has low oscillator strength).

Brennaman et al.[8] used variable-temperature studies to probe different states, as the change in temperature changed which state was enthalpically favored. Variable-temperature lifetime studies were carried out for a selection of these compounds, shown in Figure 11 for $[Re(CO)_3(dppzBr_2)(py)]PF_6$, $[Re(CO)_3(dppzBr(CF_3))(py)]PF_6$, and $[Re(CO)_3(pppBr)(py)]PF_6$.

Figure 12 shows ΔOD spectra for $[Re(CO)_3(dppzBr_2)(py)]PF_6$ at 278 and 298 K; since these are the same shape and only change a little in intensity, this indicates the same state is being probed at both temperatures. The spectrum recorded at the lower temperature is more intense because the excited state becomes easier to populate as the temperature is decreased. The transient species has its absorption maximum around 550 nm, with a shoulder at approximately 620 nm, in contrast to the ground state which has its absorption maximum around 380 nm with a tailing shoulder terminating around 500 nm.

Transient Resonance Raman. TR^2 uses the leading edge of a pulse to excite the sample and the tailing edge as the probe and is inherently biased toward observation of the THEXI state.[47] It was shown that a single state was probed, and was fully populated, as log(peak intensity) versus log(laser power) plots were linear, and the absence of some ground-state features in TR^2 spectra shows the species probed is indeed an excited state.[48] Figure 13 shows TR^2 spectra for the $dppzBr_2$ set of compounds and triplet-state frequency calculations for the Re(I) complexes. As observed by Walsh et al.,[32] the ligand TR^2 spectrum provides marker bands for the IL π,π^* state. For the $dppzBr_2$ set, the strongest band in the ligand spectrum is at 1398 cm^{-1}. This band is observed in the TR^2 spectra of both the complexes. However, these also show changes in other bands and bands that are not present in the ligand spectrum. In particular, a 1422 cm^{-1} band, which is present but very weak in the ligand spectrum, becomes the most intense band in complex spectra; a 1446 cm^{-1} band is also observed that is not present in the ligand spectrum. In Figure 13, it can be observed that the spectrum of the $[Re(CO)_3(dppzBr_2)(py)]^+$ complex resembles that of the ligand more closely than $[Re(CO)_3(dppzBr_2)Cl]$ does, indicating there is likely a greater contribution from an IL $\pi\pi^*$ state to the THEXI state for the py than chloro complex. The same is true for the other complexes studied (see Figure S14, Supporting Information). The calculated singly occupied molecular orbitals (SOMOs) of the lowest energy triplet state are shown in Figure 14. These show that the lowest energy triplet state is predicted to be MLCT(phz) in nature for both complexes; however, Figure 13 shows there is relatively poor correlation between experimental and calculated spectra, and hence, vibrational bands cannot be assigned to specific parts of the molecule using DFT calculations. Predicted spectra for the lowest energy triplet state are scaled by 0.975 because this is not necessarily the state probed in TR^2; therefore, the scale factor cannot be optimized by minimizing the MAD. As observed by Walsh et al.[32] for $[Re(CO)_3(dppzBr)Cl]$, it is likely that the triplet state has both IL π,π^* and MLCT character. The other ligands and complexes behave in a similar fashion, with LC marker bands observed in complex spectra, along with other bands present only in the spectra of complexes, which may be indicative of an MLCT state. In contrast to that observed by Walsh et al., the ligands do not all show the same IL marker band (at 1382 cm^{-1}); instead the strongest ligand TR^2 bands shift from 1344 cm^{-1} for

dx.doi.org/10.1021/ic403056g | Inorg. Chem. 2014, 53, 3126−3140

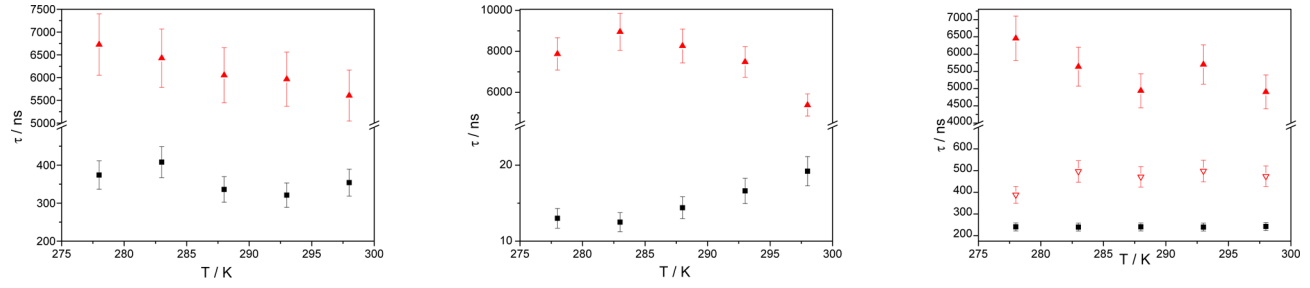

Figure 11. Variable-temperature emission and absorption lifetimes at 355 nm for (a) $[Re(CO)_3(dppzBr_2)(py)]PF_6$, (b) $[Re(CO)_3(dppzBr(CF_3))(py)]PF_6$, and (c) $[Re(CO)_3(pppBr)(py)]PF_6$. Key: (■) emission lifetimes, (▲) absorption lifetimes. For $[Re(CO)_3(pppBr)(py)]^+$, (▽) short component of the absorption lifetime. Error bars show ±10%.

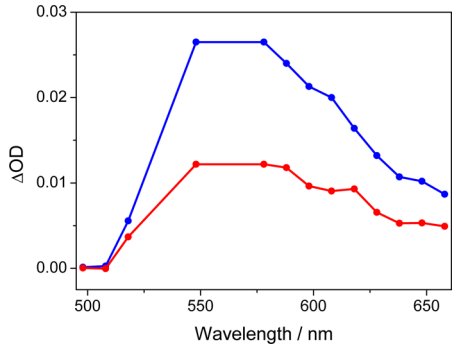

Figure 12. Variable-temperature transient absorption spectra for $[Re(CO)_3(dppzBr_2)(py)]PF_6$ at 298 K (red) and 278 K (blue).

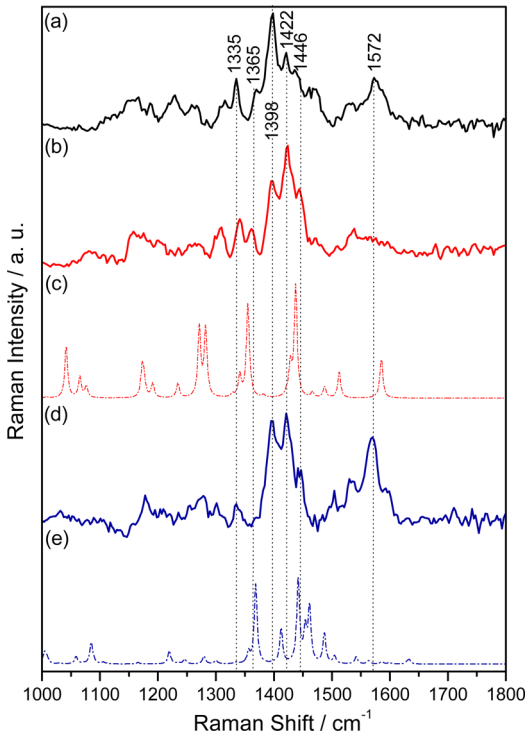

Figure 13. TR^2 spectra at 355 nm of (a) $dppzBr_2$, (b) $[Re(CO)_3(dppzBr_2)Cl]$, and (d) $[Re(CO)_3(dppzBr_2)(py)]PF_6$; predicted spectra for lowest energy triplet state of (c) $[Re(CO)_3(dppzBr_2)Cl]$, (e) $[Re(CO)_3(dppzBr_2)(py)]^+$. Samples were recorded in CH_2Cl_2 solution at concentrations of approximately 1 mM. DFT calculated lowest energy triplet states were modeled in vacuo with B3LYP functional.

$dppzBr(CF_3)$ to 1397 cm^{-1} for $dppzBr_2$, indicating the THEXI state is likely to be influenced by substituent and, therefore, probably has some phenazine nature.

Time-Resolved Infrared Spectroscopy. We have investigated further the nature of the THEXI state using TRIR spectroscopy. All observed ground- and excited-state peak positions are summarized in Table 8. Figure 15 shows the ps-TRIR spectra of $[Re(CO)_3(dppzBr)Cl]$ and $[Re(CO)_3(dppzBr_2)Cl]$ at selected times after photolysis at 400 nm. Immediately after photolysis, parent bleaches are observed at the same time as the appearance of broad excited state features. For $[Re(CO)_3(dppzBr)Cl]$ the new peaks are at ca. 2077, 2062, 2007, and 1970 cm^{-1}. Both peaks at 2077 cm^{-1} and 2062 cm^{-1} increase in intensity over the first 5−10 ps; however, the former does to a much greater extent. The final peak wavenumber values are indicative of MLCT transitions to the phen (2062 cm^{-1}) and phz (2077 cm^{-1}) orbitals on the dppz ligand. As established in literature, ν(CO) increases due to a loss of electron density in the carbonyl antibonding orbitals that is associated with MLCT transitions, where the magnitude of the change in ν(CO) can be indicative of the magnitude of the electron shift.[4,15,46,49,49−53] The excited state peaks are not stable and decay with a lifetime of 1200 ps, concurrent with the reformation of the parent bleach. In this regard, the observed photophysics are similar to the complex $[Re(CO)_3(dppzF_2)Cl]$, where MLCT states based on the phen and phz portions of the ligands were found to decay in equilibrium with a lifetime of ca. 3000 ps.[4] Closer analysis of the early time kinetics reveals a decrease in the signal intensity at around 2017 and 1877 cm^{-1}. This happens over the course of 10 ps, which matches well with the intensity increases of the MLCT peaks. This is consistent with an initially formed short-lived IL π,π^* state that converts to MLCT(phz) in the first few picoseconds of the experiment. Indeed, the parent bleaches at 1922 and 1900 cm^{-1}, which are expected to overlap significantly with the low energy carbonyl stretches of a IL π,π^* state, appear to intensify with the same kinetics. Conversely, the high energy bleach appears at its maximum intensity within the time resolution of the experiment. The excited state IR features for complexes $[Re(CO)_3(dppzBr_2)Cl]$, $[Re(CO)_3(pppBr)Cl]$, and $[Re(CO)_3(dppzBr(CF_3))Cl]$ are similar. Representative spectral features and the associated kinetics of the complex $[Re(CO)_3(dppzBr_2)Cl]$ are shown in Figure 15b and Figure 16 respectively. As with the dppzBr complex, upon photolysis parent depletions and broad peaks that are red-shifted with respect to these are observed. Again the peaks are broad, and

dx.doi.org/10.1021/ic403056g | Inorg. Chem. 2014, 53, 3126−3140

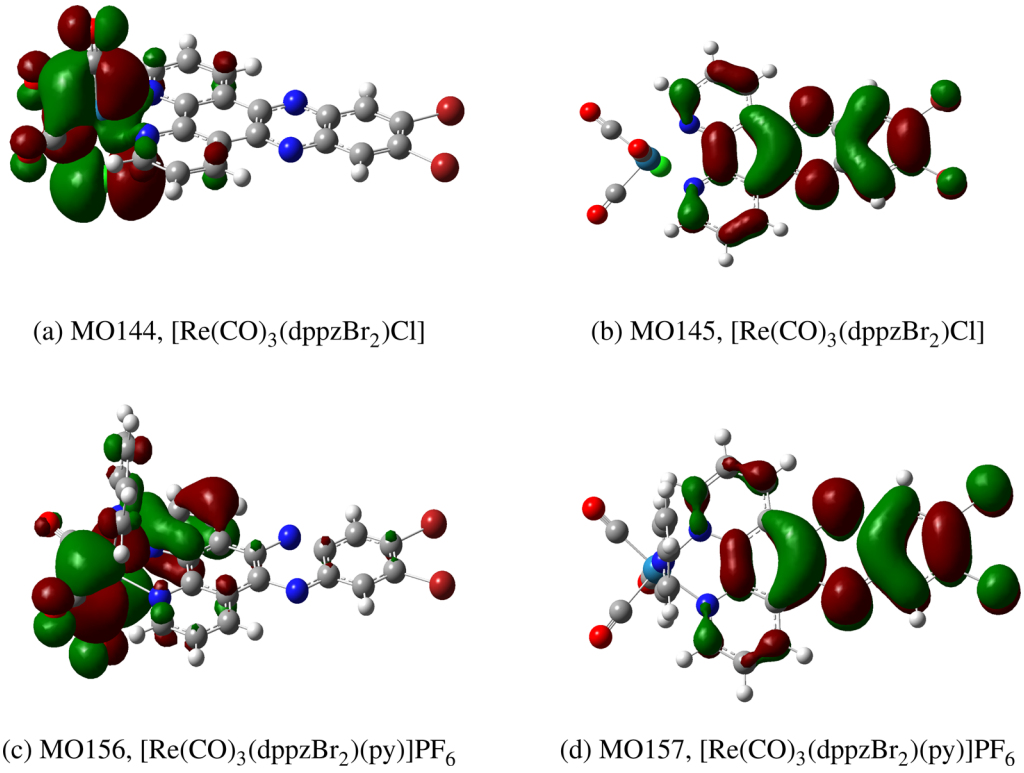

(a) MO144, $[Re(CO)_3(dppzBr_2)Cl]$ (b) MO145, $[Re(CO)_3(dppzBr_2)Cl]$

(c) MO156, $[Re(CO)_3(dppzBr_2)(py)]PF_6$ (d) MO157, $[Re(CO)_3(dppzBr_2)(py)]PF_6$

Figure 14. Singly occupied molecular orbitals for $[Re(CO)_3(dppzBr_2)Cl]$ and $[Re(CO)_3(dppzBr_2)(py)]PF_6$ calculated in vacuo with B3LYP functional.

Table 8. Summary of IR Peak Positions in the ν(CO) Stretching Region[a]

compound	ν(CO) (cm^{-1})	Assignment
$[Re(CO)_3(dppzBr_2)Cl]$	2060	MLCT(phen)
	2080, 2011, 1975	MLCT(phz)
	2026, 1925, 1901	GS
$[Re(CO)_3(dppzBr)Cl]$	2062, 1991	MLCT(phen)
	2077, 2007, 1970	MLCT(phz)
	2025, 1923, 1901	GS
$[Re(CO)_3(dppzBr(CF_3))Cl]$	2063	MLCT(phen)
	2080, 2011, 1975	MLCT(phz)
	2026, 1925, 1901	GS
$[Re(CO)_3(pppBr)Cl]$	2058, 1996	MLCT(phen)
	2082, 2011, 1975	MLCT(phz)
	2025, 1924, 1901	GS
$[Re(CO)_3(dppzBr_2)(py)]^+$	2072	MLCT(phen)
	2035, 1921	IL π,π^*
	2039, 1935	GS
$[Re(CO)_3(dppzBr)(py)]^+$	2078	MLCT(phen)
	2035, 1922	IL π,π^*
	2039, 1937	GS
$[Re(CO)_3(dppzBrCF_3)(py)]^+$	2039, 1925	IL π,π^*
	2041, 1936	GS
$[Re(CO)_3(pppBr)(py)]^+$	2076, 1979	MLCT(phen)
	2036, 1913	IL π,π^*
	2040, 1938	GS

[a]All experiments were carried out in CH_2Cl_2, with 400 nm excitation.

sharpening as well as a shift to higher wavenumbers occurs over the first 10−20 ps. This can be assigned either to vibrational cooling or a MLCT(phen) to MLCT(phz) conversion. The retention of a shoulder to low energies of the 2077 cm^{-1} excited state peak indicates that both MLCT(phen) and MLCT(phz) states are present, which exist in equilibrium. This equilibrium appears to lie toward MLCT(phz), as the corresponding vibrational peak is dominant, which is particularly evident for the complexes $[Re(CO)_3(dppzBr(CF_3))Cl]$ and $[Re(CO)_3(dppzBr)Cl]$. This implies that the dppz(phz) orbitals are more stabilized for these complexes, which is not unexpected when considering that they possess the highest reduction potentials (vide supra) and thus the most electron-deficient dppz(phz) orbitals.

The ps-TRIR spectra of $[Re(CO)_3(dppzBr_2)(py)]^+$ are shown in Figure 17. Bleaching of the parent bands occurs immediately after photolysis, and several excited state peaks appear. A set of bands are present to lower energies, consistent with the formation of an IL π,π^* state. These bands blue-shift to their final positions of 2035 and 1921 cm^{-1} over the course of ca. 30 ps. This observation is consistent with the process of vibrational cooling. These peaks are stable for the duration of the experiment, consistent with the observations made in transient absorption experiments (vide supra). In addition to the IL π,π^* peaks a band is observed at 2072 cm^{-1}, which is indicative of a MLCT state, as discussed above. This band appears to grow in over the first 5 ps of the experiment; however, little or no blue-shifting can be observed. The magnitude of the shift of the band is indicative of localization of the excited state electron on the phen orbital of the dppz ligand. Due to the low intensity of the MLCT band it is difficult to determine whether the initial kinetics are due to vibrational cooling or conversion from a different excited state. This band decays with a lifetime of 1.3 ns. Similar observations can be made for the remaining $[Re(CO)_3(L)(py)]$+ complexes. Just as for $[Re(CO)_3(dppzBr_2)(py)]^+$, initially formed IL π,π^* marker bands blue-shift in the first 20−30 ps and remain for the

dx.doi.org/10.1021/ic403056g | Inorg. Chem. 2014, 53, 3126−3140

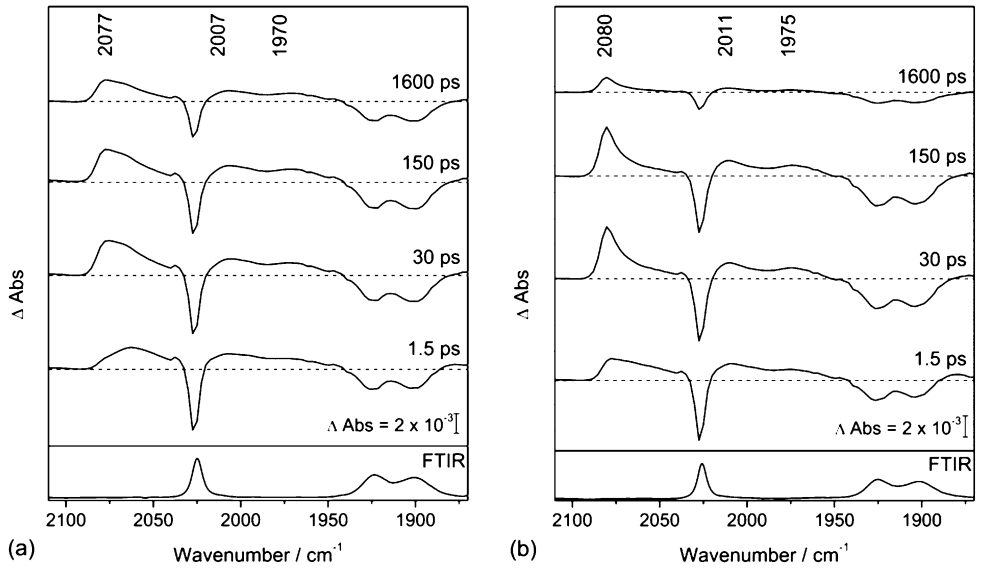

Figure 15. ps-TRIR spectra at selected time-delays after photolysis with a 400 nm pulse, acquired in CH_2Cl_2: (a) $[Re(CO)_3(dppzBr)Cl]$, (b) $[Re(CO)_3(dppzBr_2)Cl]$.

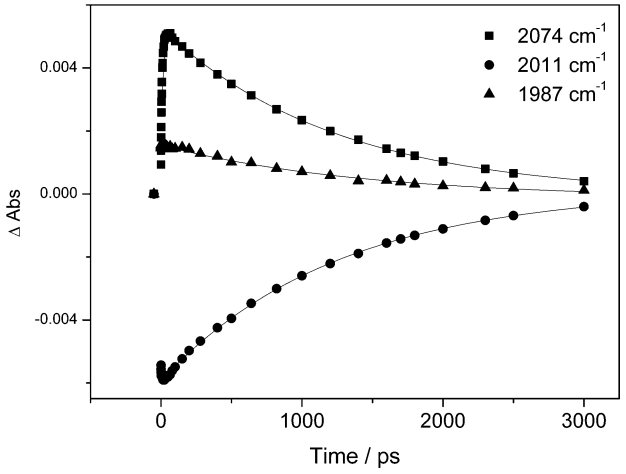

Figure 16. Fitted exponential decays of prominent features in the ps-TRIR spectra of $[Re(CO)_3(dppzBr_2)Cl]$ acquired in CH_2Cl_2.

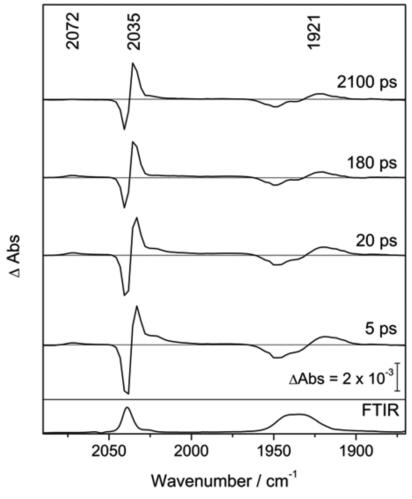

Figure 17. ps-TRIR spectra of $[Re(CO)_3(dppzBr_2)(py)]^+$, acquired in CH_2Cl_2, after photolysis using a 400 nm pulse.

duration of the ps experiments (see Table 8 for accurate positions). However, the MLCT(phen) bands show different behavior. For $[Re(CO)_3(dppzBr(CF_3))(py)]^+$ no discernible MLCT band can be observed throughout the ps or ns time scales (see Figure S15(a), Supporting Information). $[Re(CO)_3(dppzBr)(py)]^+$ shows a very weak band centered at 2078 cm^{-1}, which grows in over the first 5 ps of the experiment, followed by decay with a lifetime of 530 ps (see Figure S15(b), Supporting Information). Similarly, $[Re(CO)_3(pppBr)(py)]^+$ (see Figure S15(c), Supporting Information) shows fast growth of a MLCT band; however, it is stable until the end of the ps experiment. No evidence for localization of the MLCT state on the phz portion of the ligand can be observed on these time scales. Common to all complexes is the presence of a feature at ca. 2026 cm^{-1} in the early ps spectra (see Figure 17 for an example). A similar observation has been made for the complex $[Re(CO)_3(dppz)(py\text{-}R)]$, (R is a nonconjugated link to a fragment of DNA) by Olmon et al.[54] who have assigned it as a breakdown product. While this is a possible assignment it should be noted that the decay times of these bands match well with the processes assigned as vibrational cooling above. The presence of additional short-lived excited states, for example involving the ancillary py ligands, can therefore not be ruled out; further experiments, such as the investigation of the fingerprint region on the ultrafast time scale, are required to make a more definitive assignment.

CONCLUSION

The synthesis and characterization of a series of dppz ligands substituted with electron-withdrawing groups and their $[Re(CO)_3(L)Cl]$ and $[Re(CO)_3(L)(py)]PF_6$ complexes are reported. Crystal structures of $[Re(CO)_3(dppzBr_2)Cl]$ and $[Re(CO)_3(dppzBr)(py)]PF_6$ are reported, while other calculated structures are verified by comparison of experimental and calculated vibrational spectra. The Franck−Condon state was probed using resonance Raman spectroscopy and interpreted using TD-DFT calculations, and it showed that ligand centered $\pi \rightarrow \pi^*$(phz) transitions are observed between 350 and 390 nm for complexes and MLCT transitions as a tailing shoulder out to approximately 500 nm. The MLCT state is localized to the

dx.doi.org/10.1021/ic403056g | Inorg. Chem. 2014, 53, 3126−3140

phen MO for all complexes except $[Re(CO)_3(dppzBr_2)Cl]$, $[Re(CO)_3(pppBr)Cl]$, and $[Re(CO)_3(pppBr)(py)]^+$, for which there appears to be a mixed MLCT phen/phz state. Complexes are weakly emissive in CH_2Cl_2, and emission is short, decaying in >10 ns with the laser pulse for most complexes. Transient absorption shows dark states for most complexes with appreciable lifetimes (μs). Transient resonance Raman and time-resolved infrared spectroscopy have been used to investigate the natures of the THEXI states of these complexes. It was found that the $[Re(CO)_3(L)Cl]$ complexes possess MLCT states based on the phen and phz portions of the dppz ligands, which show a phen to phz shift to give an equilibrium. The position of this equilibrium correlates qualitatively with the reduction potentials of the ligands. Consistent with transient absorption and emission spectroscopic techniques, the excited states decay within several nanoseconds. Conversely, the $[Re(CO)_3(L)(py)]^+$ complexes show long-lived IL π,π^* excited states, in agreement with transient absorption results. Furthermore, several of these complexes showed relatively short-lived MLCT(phen) states. TR^2 spectra are less definitive but suggest that $[Re(CO)_3(L)(py)]^+$ complexes have a greater contribution to the THEXI state from an IL π,π^* state since spectra resemble those of the relevant ligand more closely than $[Re(CO)_3(L)Cl]$ complexes; this is consistent with TRIR data.

■ ASSOCIATED CONTENT

Supporting Information

Scale factors and MAD values, experimental and calculated FT-Raman spectra, vibrational band assignments, modeled vibrational mode pictures, resonance Raman spectra, TR^2 spectra, and TRIR spectra of $[Re(CO)_3(py)(L)]^+$ compounds where L = dppzBr(CF_3), dppzBr, and pppBr. This material is available free of charge via the Internet at http://pubs.acs.org/.

■ AUTHOR INFORMATION

Corresponding Authors

*E-mail: mike.george@nottingham.ac.uk. (M.W.G.) Phone: +64 (3)4797599. Fax: +64 (3)4797906.

*E-mail: keith.gordon@otago.ac.nz. (K.C.G.)

Notes

The authors declare no competing financial interest.

■ ACKNOWLEDGMENTS

M.W.G. gratefully acknowledges receipt of a Wolfson Merit Award.

■ REFERENCES

(1) Amouyal, E.; Homsi, A.; Chambron, J.-C.; Sauvage, J.-P. *Dalton Trans.* **1990**, *6*, 1841−1845.

(2) Fees, J.; Kaim, W.; Moscherosch, M.; Matheis, W.; Klima, J.; Krejcik, M.; Zalis, S. *Inorg. Chem.* **1993**, *32*, 166−174.

(3) Kuhnt, C.; Tschierlei, S.; Karnahl, M.; Rau, S.; Dietzek, B.; Schmitt, M.; Popp, J. *J. Raman Spectrosc.* **2010**, *41*, 922−932.

(4) Kuimova, M. K.; Alsindi, W. Z.; Blake, A. J.; Davies, E. S.; Lampus, D. J.; Matousek, P.; McMaster, J.; Parker, A. W.; Towrie, M.; Sun, X.-Z.; Wilson, C.; George, M. W. *Inorg. Chem.* **2008**, *21*, 9857−9869.

(5) Arias, M.; Concepcion, J.; Crivelli, I.; Delgadillo, A.; Diaz, R.; Francois, A.; Gajardo, F.; Lopez, R.; Leiva, A. M.; Loeb, B. *Chem. Phys.* **2006**, *326*, 54−70.

(6) Kalyanasundaram, K.; Grätzel, M. *Coord. Chem. Rev.* **1998**, *77*, 347−414.

(7) Friedman, A. E.; Chambron, J.-C.; Sauvage, J.-P.; Turro, N. J.; Barton, J. K. *J. Am. Chem. Soc.* **1990**, *112*, 4960−4962.

(8) Brennaman, M. K.; Alstrum-Acevedo, J. H.; Fleming, C. N.; Jang, P.; Meyer, T. J.; Papanikolas, J. M. *J. Am. Chem. Soc.* **2002**, *124*, 15094−15098.

(9) Li, J.; Chen, J.-C.; Xu, L.-C.; Zheng, K.-C.; Ji, L.-N. *J. Organomet. Chem.* **2007**, *692*, 831−838.

(10) Horvath, R.; Otter, A. M.; Ainscough, E. W. *Inorg. Chem.* **2010**, *49*, 4073.

(11) Stoeffler, H. D.; Thornton, N. B.; Temkin, S. L.; Schanze, K. S. *J. Am. Chem. Soc.* **1995**, *117*, 7119−7128.

(12) Schoonover, J. R.; Bates, W. D.; Meyer, T. J. *Inorg. Chem.* **1995**, *34*, 6421−6422.

(13) Schoonover, J. R.; Strouse, G. F.; Dyer, R. B.; Bates, W. D.; Chen, P.; Meyer, T. J. *Inorg. Chem.* **1996**, *35*, 273−274.

(14) Atsumi, M.; Gonzalez, L.; Daniel, C. *J. Photochem. Photobiol., A* **2007**, *190*, 310−320.

(15) Horvath, R.; Gordon, K. C. *Inorg. Chim. Acta* **2011**, *374*, 10−18.

(16) Suzuki, A. *Angew. Chem., Int. Ed.* **2011**, *50*, 6722−6737.

(17) Lundin, N. J.; Walsh, P. J.; Howell, S. L.; McGarvey, J. J.; Blackman, A. G.; Gordon, K. C. *Inorg. Chem.* **2005**, *44*, 3551−3560.

(18) Fraser, M. G. The Synthesis and Spectroscopic Properties of Some Rhenium(I) and Copper(I) Polypyridyl Complexes. Ph.D. Thesis, University of Otago, 2012.

(19) Howell, S. L.; Gordon, K. C. *J. Phys. Chem. A* **2004**, *108*, 2536−2544.

(20) Lind, S. J.; Gordon, K. C.; Waterland, M. R. *J. Raman Spectrosc.* **2008**, *39*, 1556−1567.

(21) Lind, S. J.; Walsh, T. J.; Blackman, A. G.; Polson, M. I. J.; Irwin, G. I. S.; Gordon, K. C. *J. Phys. Chem. A* **2009**, *15*, 3566−3575.

(22) Horvath, R.; Fraser, M. G.; Cameron, S. A.; Blackman, A. G.; Wagner, P.; Officer, D. L.; Gordon, K. C. *Inorg. Chem.* **2013**, *52*, 1304−1317.

(23) Towrie, M.; David, C.; Dyer, J.; Weinstein, J. A.; Matousek, P.; Barton, R.; Bailey, P. D.; Subramaniam, N.; Kwok, W. M.; Ma, C.; Phillips, D.; Parker, A. W.; George, M. W. *Appl. Spectrosc.* **2003**, *59*, 367.

(24) Frisch, M. J. et al. Gaussian 09 Revision A.02, Gaussian Inc., Wallingford, CT, 2009.

(25) Horvath, R.; Gordon, K. C. *Coord. Chem. Rev.* **2010**, *254*, 2505−2518.

(26) Schaftenaar, G.; Noordik, J. *J. Comput. Aided Mol. Des.* **2000**, *14*, 123−134.

(27) Cleland, D. M.; Irwin, G.; Wagner, P.; Officer, D. L.; Gordon, K. C. *Chem.—Eur. J.* **2009**, *15*, 3682−3690.

(28) Lundin, N. J.; Walsh, P. J.; Howell, S. L.; Blackman, A. G.; Gordon, K. C. *Chem.—Eur. J.* **2008**, *14*, 11573−11583.

(29) Lundin, N. J.; Blackman, A. G.; Gordon, K. C.; Officer, D. L. *Angew. Chem., Int. Ed.* **2006**, *45*, 2582−2584.

(30) Howell, S. L.; Gordon, K. C.; Waterland, M. R.; Leung, K. H.; Phillips, D. L. *J. Phys. Chem. A* **2006**, *110*, 11194−11199.

(31) Horvath, R.; Otter, C. A.; Gordon, K. C.; Brodie, A. M.; Ainscough, E. W. *Inorg. Chem.* **2010**, *49*, 4073−4083.

(32) Walsh, P. J.; Gordon, K. C.; Lundin, N. J.; Blackman, A. G. *J. Phys Chem. A* **2005**, *109*, 5933−5942.

(33) Scott, A. P.; Radom, L. *J. Phys. Chem.* **1996**, *100*, 16502−16513.

(34) Earles, J. C.; Gordon, K. C.; Officer, D. L.; Wagner, P. *J. Phys. Chem. A* **2007**, *111*, 7171−7180.

(35) Earles, J. C.; Gordon, K. C.; Stephenson, A. W. I.; Partridge, A. C.; Officer, D. L. *Phys. Chem. Chem. Phys.* **2011**, *13*, 1597−1605.

(36) Noviandri, I.; Brown, K.; Fleming, D.; Gulyas, P.; Lay, P. A.; Masters, A. F.; Phillips, L. *J. Phys. Chem. B* **1999**, *103*, 6713−6722.

(37) Bard, A. J., Faulkner, L., Eds. *Electrochemical Methods: Fundamentals and Applications*, 2nd ed.; John Wiley and Sons, Inc.: New York, 2001.

(38) Matthewson, B. J.; Flood, A.; Polson, M. I. J.; Armstrong, C.; Phillips, D. L.; Gordon, K. C. *Bull. Chem. Soc. Jpn.* **2002**, *75*, 933−942.

(39) Dyer, J.; Blau, W. J.; Coates, C. G.; Creely, C. M.; Gavey, J. D.; George, M. W.; Grills, D. C.; Hudson, S.; Kelly, J. M.; Matousek, P.; McGarvey, J. J.; McMaster, J.; Parker, A. W.; Towrie, M.; Weinstein, J. A. *Photochem. Photobiol. Sci.* **2003**, *2*, 542−554.

(40) Vlček, A.; Záliš, S. *Coord. Chem. Rev.* **2007**, *251*, 258−287.
(41) Waterland, M. R.; Gordon, K. C.; McGarvey, J. J.; Jayaweera, P. M. *Dalton Trans.* **1998**, *4*, 609−616.
(42) DeArmond, M. K.; Hanck, K. W.; Wertz, D. W. *Coord. Chem. Rev.* **1985**, *64*, 65−81.
(43) Stoyanov, S. R.; Villegas, J. M.; Cruz, A. J.; Lockyear, L. L.; Reibenspies, J. H.; Rillema, D. P. *J. Chem. Theory Comput.* **2005**, *1*, 95−106.
(44) Clark, R. J. H.; Dines, T. J. *Angew. Chem., Int. Ed.* **1986**, *25*, 131−158.
(45) Hirakawa, A. Y.; Tsuboi, M. *Science* **1975**, *188*, 359−361.
(46) Kuimova, M. K.; Alsindi, W. Z.; Dyer, J.; Grills, D. C.; Jina, O. S.; Matousek, P.; Parker, A. W.; Portius, P.; Sun, X. Z.; Towrie, M.; Wilson, C.; Yang, J.; George, M. W. *Dalton Trans.* **2003**, 3996−4006.
(47) Babcock, G. T.; Jean, J. M.; Johnston, L. N.; Palmer, G.; Woodruff, W. H. *J. Am. Chem. Soc.* **1984**, *106*, 8305−8306.
(48) Al-Obaidi, A. H. R.; Gordon, K. C.; McGarvey, J. J.; Bell, S. E. J.; Grimshaw, J. *J. Phys. Chem.* **1993**, *97*, 10942−10947.
(49) Busby, M.; Matousek, P.; Towrie, M.; Vlcek, A. *J. Phys. Chem. A* **2005**, *109*, 3000−3008.
(50) Butler, J. M.; George, M. W.; Schoonover, J. R.; Dattelbaum, D. M.; Meyer, T. J. *Coord. Chem. Rev.* **2007**, *251*, 492−514.
(51) Dyer, J.; Creely, C. M.; Penedo, J. C.; Grills, D. C.; Hudson, S.; Matousek, P.; Parker, A. W.; Towrie, M.; Kelly, J. M.; George, M. W. *Photochem. Photobiol. Sci.* **2007**, *6*, 741.
(52) George, M. W.; Johnson, F. P. A.; Westwell, J. R.; Hodges, P. M.; Turner, J. J. *Dalton Trans.* **1993**, *19*, 2977.
(53) Kuimova, M. K.; Sun, X. Z.; Matousek, P.; Grills, D. C.; Parker, A. W.; Towrie, M.; George, M. W. *Photochem. Photobiol. Sci.* **2007**, *6*, 1158−1163.
(54) Olmon, E. D.; Sontz, P. A.; Blanco-Rodriguez, A. M.; Towrie, M.; Clark, I. P.; Vlcek, A.; Barton, J. K. *J. Am. Chem. Soc.* **2011**, *133*, 13718.